INTERNATIONAL JOURNAL FOR NUMERICAL METHODS IN FLUIDS, VOL. 20, 507–522 (1995)

NUMERICAL STUDY OF RADIATIVE IGNITION OF PYROLYSING SOLID FUELS

P. DURBETAKI

The George W. Woodruff School of Mechanical Engineering, Georgia Institute of Technology, Atlanta, GA 30332-0405, U.S.A.

T. X. PHUOC, M. P. MATHUR AND J. M. EKMANN

U. S. Department of Energy, Pittsburgh Energy Technology Center, P. O. Box 10940; MS: 84-30, Pittsburgh, PA 15236, U.S.A.

SUMMARY

A numerical model of radiative ignition of pyrolysing solid fuels is developed. The model is one-dimensional and transient. The following mechanisms are simultaneously accounted for: (i) the surface heat and mass transport, (ii) the surface oxidation chemical reaction, (iii) the in-depth pyrolysis, (iv) the gas-phase heating by absorption of the radiation and by heat conduction/convection from the solid surface, and (v) the gas-phase chemical reaction. The solutions are obtained numerically with the method of lines. Using lignite and bituminous coal for the simulations, the results confirm that the pyrolysis products absorb a significant amount of the external radiation. Predictions of the ignition times show that both the surface ignition time and the gas-phase ignition time decrease rapidly with increasing radiation intensities. A good agreement between predictions and experiments is obtained.

A sensitivity analysis is also carried out with the key kinetic parameters. This analysis establishes an upper limit for surface and pyrolysis activation energies and a lower limit for gas-phase activation energy. Within these limits, the radiative ignition of coals appears as an integration of two consecutive ignition modes: the surface ignition occurs first, which is then followed by the gas-phase ignition. Beyond these limits, the single gas-phase ignition mode is the only ignition mode to prevail.

KEY WORDS: radiative ignition; pyrolysing solid fuels; coal; numerical model; numerical method of lines

1. INTRODUCTION

Radiative ignition of a pyrolysing solid fuel has been studied extensively in the past. This subject is of interest in many practical situations such as fire safety, power generation, solid waste treatment, etc. It has been shown experimentally that when a pyrolysing solid fuel is exposed to a radiative heat source, a significant amount of the external radiation flux is absorbed by the pyrolysis products during the early stages of the ignition period.[1–3] This important feature is believed to lead to a series of non-linear phenomena that dictate complex interactions among simultaneous but different processes such as heat transfer, mass transfer and chemical reactions.

Some theoretical investigations are also available.[4–11] Some of these studies,[3–7] are limited only to the case of the effect of the absorption of radiation on the gas-phase ignition. Other studies,[8–11] extend the analysis to include the contribution of the surface ignition reaction during the ignition event. For some solids, such as coal, such a contribution is important as it results in surface ignition at high oxygen concentration and/or small particle size.[12]

CCC 0271–2091/95/060507–16

Received 10 March 1994
Revised 2 November 1994

The main objective of the present work is to develop a numerical model, based on the method of lines, to calculate the ignition of a pyrolysing solid material suddenly exposed to a radiative heating source. The model is one-dimensional, transient, and incorporates the following: the surface ignition reaction, the in-depth pyrolysis, the gas-phase absorption of the radiation by the pyrolysis products, and the gas-phase chemical reaction. A sensitivity analysis is also performed to determine the dependence of the ignition phenomena on the kinetic parameters.

2. THE NUMERICAL MODEL

A sketch of various steps in developing the present model are shown in Figure 1. A one-dimensional pyrolysing solid fuel, initially at ambient temperature, is heated by a radiative heat source. As the temperature of the solid fuel increases, both the surface oxidation chemical reaction and the in-depth volatile production ensue. The volatile gases escape from the fuel surface and mix with oxidant in the gas phase. Simultaneously, the volatile gases also absorb some of the radiation which in turn heat the gas phase rapidly. Under appropriate conditions, these processes are followed by ignition. Depending on the competition among these processes, the ignition may appear as a single gas-phase ignition mode or as an integration of two consecutive ignition modes. The former results if the surface ignition reaction does not have enough time to develop before the devolatilization temperature is reached, and the latter is obtained if the surface ignition reaction has enough time to develop before a strong production of volatile gases is achieved. The numerical model, therefore, takes into account simultaneously the processes mentioned above.

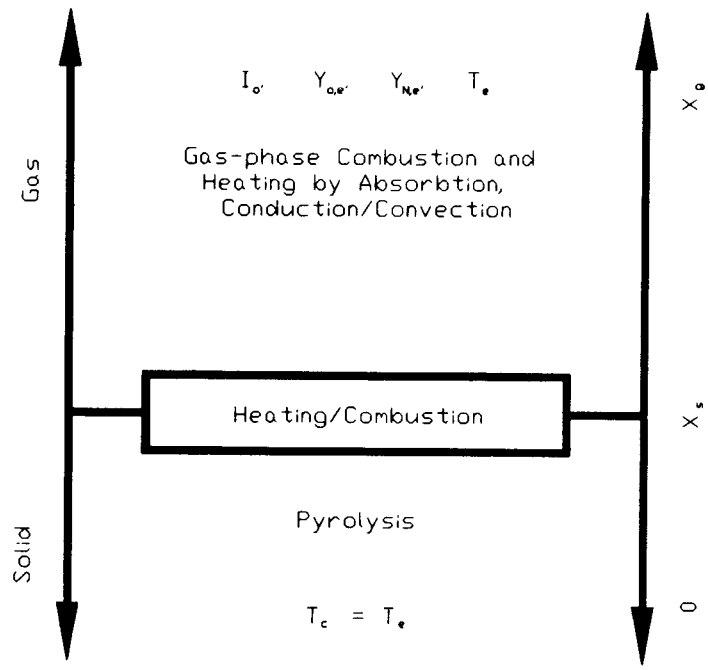

Figure 1. The physical model of radiative ignition of a pyrolysing solid fuel

3. FORMULATION

3.1. Assumptions

The governing equations are simplified subject to the following assumptions:

(i) The process is one-dimensional and transient; the flow in the gas phase is laminar; the external pressure is constant and the gas mixture behaves like a perfect gas. Molecular weights of all species are constant and equal; the Lewis number is unity.
(ii) The thermophysical properties, $\rho^2 D$, and $\rho_g \lambda_g$ are constant.
(iii) The solid oxidation reaction occurs only at the surface and is described by a first-order finite rate Arrhenius equation; the pyrolysis process occurs volumetrically and is described by a zero-order finite rate Arrhenius equation; the gas-phase reaction is described by a second-order finite rate Arrhenius equation.
(iv) The absorption of the radiation by the solid occurs at the solid surface; Beer's law is used for the absorption of the radiation by the gas phase and the absorption coefficient is proportional to the sum of mass fraction of the pyrolysis gases and the combustion product gases.
(v) The effects of natural convection are neglected.

3.2. Conservation equations

For the model under consideration, the derived conservation equations are

gas phase mass

$$\frac{\partial \rho_g}{\partial t} + \frac{\partial (\rho_g u)}{\partial x} = 0 \tag{1}$$

species

$$\rho_g \frac{\partial Y_i}{\partial t} + \rho_g u \frac{\partial Y_i}{\partial x} = \omega_i + \frac{\partial}{\partial x} \rho_g D \frac{\partial Y_i}{\partial x} \tag{2}$$

where i is for volatile gas, v, oxygen, O and inert gas, N,

product gas

$$Y_p = 1 - (Y_v + Y_O + Y_N) \tag{3}$$

gas phase energy

$$\rho_g c_{p,g} \left(\frac{\partial T_g}{\partial t} + u \frac{\partial T_g}{\partial x} \right) = - \omega_v \Delta H_g + \frac{\partial}{\partial x} \lambda_g \frac{\partial T_g}{\partial x} + \frac{dI}{dx} \tag{4}$$

where

$$\frac{dI}{dx} = \beta_g I_0 (Y_v + Y_p) e^{-\int_x^{x_s} \beta_g (Y_v + Y_p) dx} \tag{5}$$

equation of state

$$\rho_{g,e} T_{g,e} = \rho_g T_g \tag{6}$$

solid phase energy

$$\frac{\partial T_c}{\partial t} = \alpha_c \frac{\partial^2 T_c}{\partial x^2} - \frac{\omega_p \Delta H_v}{c_{p,c}} \tag{7}$$

The conservation equations must be solved subject to

Boundary and initial conditions

For $t < 0$, all x:

$$T_c = T_g = T_e; \quad Y_{v,c} = 0 \tag{8}$$

$$Y_v = Y_p = 0; \quad Y_i = Y_{i,e} \quad \text{with } i = O, N \tag{9}$$

For $t \geqslant 0$, and at the back of the solid; $x = 0$:

$$T_{c,0} = T_e; \quad \left(\frac{\partial T_c}{\partial x}\right)_0 = 0 \tag{10}$$

For $t \geqslant 0$, and the gas–solid interface; $x = x_s$:

$$-\lambda_c\left(\frac{\partial T_c}{\partial x}\right)_s + \beta_c I_s + \lambda_g\left(\frac{\partial T_g}{\partial x}\right)_s + H_s = 0 \tag{11}$$

where H_s is the heat transfer rate at the interface and is given by

$$H_s = \omega_c \Delta H_c - m_s c_{p,g}(T_{c,s} - T_g) - \beta_s \sigma T_{c,s}^4 \tag{12}$$

$$T_{c,s} = T_{g,s}; \quad \left(\frac{\partial T_c}{\partial t}\right)_s = \left(\frac{\partial T_g}{\partial t}\right)_s \tag{13}$$

$$m_s Y_{O,s} = \rho_g D\left(\frac{\partial Y_O}{\partial x}\right)_s - \omega_c \tag{14}$$

$$m_s Y_{N,s} = \rho_g D\left(\frac{\partial Y_N}{\partial x}\right)_s \tag{15}$$

$$m_s(Y_{v,s} - 1) = \rho_g D\left(\frac{\partial Y_v}{\partial x}\right)_s \tag{16}$$

and

$$m_s = \rho_c \int_0^{x_s} \omega_p \, dx \tag{17}$$

For $t \geqslant 0$, $x = x_g$:

$$T_{g,e} = T_e; \quad I_e = I_0 \tag{18}$$

$$Y_{v,e} = 0; \quad Y_i = Y_{i,e} \quad \text{with } i = O, N \tag{19}$$

$$\left(\frac{\partial T_g}{\partial x}\right)_e = \left(\frac{dI}{dx}\right)_e = \left(\frac{\partial Y_i}{\partial x}\right)_e = 0 \quad \text{with } i = v, O, N \tag{20}$$

The reaction rates in the conservation equations are established through the Arrhenious constitutive equations. Thus for the gas-phase reaction of the volatile gas

$$\omega_v = -A_g v_v M_v Y_v Y_O \rho_g^2 e^{-E/RT_g} \tag{21}$$

the consumption rate of oxygen

$$\omega_O = r_{st}\omega_v \tag{22}$$

where

$$r_{st} = \frac{v_O M_O}{v_v M_v} \tag{23}$$

the inert gas

$$\omega_N = 0 \tag{24}$$

the surface reaction rate

$$\omega_c = A_c \rho_{g,e} Y_{O,s} e^{-E_c/RT_{c,s}} \tag{25}$$

and the pyrolysis rate

$$\omega_p = A_p (Y^*_{v,c} - Y_{v,c}) e^{-E_p/RT_c} \tag{26}$$

3.3. *Transformations*

Define

$$\theta_i = \frac{T_i}{T_e} \quad \text{with } i = g, c \tag{27}$$

$$\eta = \frac{x}{x_s}; \quad \phi = \frac{I}{I_0} \tag{28}$$

$$E^*_g = \frac{E_g}{RT_e}; \quad E^*_c = \frac{E_c}{RT_e}; \quad E^*_p = \frac{E_p}{RT_e} \tag{29}$$

$$\Pi_v = -\left(\frac{A_g \nu_v M_v \rho_{g,e} Y_v Y_O e^{-E^*_g/\theta_g}}{\theta_g} \right) \tag{30}$$

$$Q_g = -\frac{\Pi_v \Delta H_g}{T_e c_{p,g}}; \quad Q_c = \frac{\omega_c \Delta H_c x_s}{T_e \lambda_c} \tag{31}$$

$$Q_I = \frac{\beta_c \phi_s I_0 x_s}{T_e \lambda_c}; \quad Q_v = \frac{m_s c_{p,g} x_s (\theta_s - 1)}{\lambda_s} \tag{32}$$

$$\Pi_1 = \frac{\rho_g \lambda_g x_s}{\lambda_c}; \quad Q_r = \frac{\beta_c \sigma T_e^3 x_s \theta^4_{c,s}}{\lambda_c} \tag{33}$$

In the gas phase, the governing equations and boundary conditions are written in the physical co-ordinate x which is highly compressed in the mixing zone. In order to maintain a uniform grid in the computational domain, the x-co-ordinate is replaced by the gas-phase stream function. The gas-phase stream function is defined to account for variables gas density, and

$$\xi(x,t) = \int_{x_s}^{x} \rho_g(x,t)\, dx \tag{34}$$

For the solid, the following relations are used

$$\frac{\partial(\ )_c}{\partial t} = \frac{\partial(\ )_c}{\partial \eta} \frac{d\eta}{dt} \tag{35}$$

$$\frac{\partial(\ )_c}{\partial x} = \frac{\partial(\ )_c}{\partial \eta} \frac{d\eta}{dx} \tag{36}$$

For the gas phase, the following relations are used

$$\frac{\partial(\ )_g}{\partial t} = \frac{\partial(\ )_g}{\partial \xi}\frac{d\xi}{dt} \tag{37}$$

$$\frac{\partial(\ )_g}{\partial x} = \frac{\partial(\ )_g}{\partial \xi}\frac{d\xi}{dx} \tag{38}$$

where

$$\frac{d\eta}{dt} = -\frac{\eta}{x_s}\frac{dx_s}{dt}; \quad \frac{d\eta}{dx} = \frac{1}{x_s} \tag{39}$$

$$\frac{d\xi}{dt} = \int_{\xi_s}^{\xi}\frac{\partial \rho_g}{\partial t}\frac{d\xi}{\rho_g} - \rho_{g,s}\frac{dx_s}{dt}; \quad \frac{d\xi}{dx} = \rho_g \tag{40}$$

The transformed conservation equations are

gas phase mass

$$\rho_g u(\xi, t) = -\int_{\xi_s}^{\xi}\frac{\partial \rho_g}{\partial t}\frac{d\xi}{\rho_g} + m_s \tag{41}$$

species

$$\frac{\partial Y_i}{\partial t} = \Pi_i + \rho_g^2 D\frac{\partial^2 Y_i}{\partial \xi^2} - m_s\frac{\partial Y_i}{\partial \xi} \quad \text{with } i = v, O, N \tag{42}$$

$\Pi_O = \Pi_v r_{st}$ and $\Pi_N = 0$.

gas phase energy

$$\frac{\partial \theta_g}{\partial t} = Q_g + \frac{\rho_g \lambda_g}{c_{p,g}}\frac{\partial^2 \theta_g}{\partial \xi^2} - m_s\frac{\partial \theta_g}{\partial \xi} + \frac{I_0}{c_{p,g}T_e}\frac{d\phi}{d\xi} \tag{43}$$

solid phase energy

$$\frac{\partial \theta_c}{\partial t} = \frac{\alpha_c}{x_s^2}\frac{\partial^2 \theta_c}{\partial \eta^2} - \frac{\omega_p \Delta H_p}{c_{p,c}T_e} \tag{44}$$

where

$$\frac{d\phi}{d\xi} = \frac{\theta_g \beta_g (Y_v + Y_p) e^{-(1/\rho_{g,e})\int_{\xi}^{\xi_s}\beta_g \theta_g (Y_v + Y_p)d\xi}}{\rho_{g,e}} \tag{45}$$

and

$$m_s = \rho_c x_s \int_0^1 \omega_p d\eta \tag{46}$$

Boundary and initial conditions

For $t < 0$:

$$\theta_c = \theta_g = 1; \quad Y_{v,c} = 0 \tag{47}$$

For $t \geqslant 0$, $\eta = 0$:

$$\theta_{c,0} = 1; \quad \left(\frac{\partial \theta_c}{\partial \eta}\right)_0 = 0 \tag{48}$$

For $t \geqslant 0$, $\eta = 1$ and $\xi = \xi_s$:

$$\phi_s = \phi_s(t) \tag{49}$$

$$\theta_{c,\eta=1} = \theta_{g,\xi_s}; \quad \left(\frac{\partial\theta_c}{\partial t}\right)_{\eta=1} = \left(\frac{\partial\theta_g}{\partial t}\right)_{\xi=\xi_s} \tag{50}$$

$$-\left(\frac{\partial\theta_c}{\partial\eta}\right)_{\eta=1} + \Pi_1\left(\frac{\partial\theta_g}{\partial\xi}\right)_{\xi=\xi_s} + Q_I + Q_c - Q_v - Q_r = 0 \tag{51}$$

$$m_s Y_{O,s} = \rho_g^2 D\left(\frac{\partial Y_O}{\partial\xi}\right)_{\xi=\xi_s} - \omega_c \tag{52}$$

$$m_s Y_{N,s} = \rho_g^2 D\left(\frac{\partial Y_N}{\partial\xi}\right)_{\xi=\xi_s} \tag{53}$$

$$Y_{v,s} = 1 + \frac{\rho_g^2 D}{m_s}\left(\frac{\partial Y_v}{\partial\xi}\right)_{\xi=\xi_s} \tag{54}$$

For $t \geqslant 0$ and at $\xi = \xi_g$:

$$Y_{v,e} = 0; \quad Y_i = Y_{i,e} \quad \text{with } i = O, N \tag{55}$$

$$\theta_{g,e} = \phi_e = 1{\cdot}0 \tag{56}$$

$$\left(\frac{\partial\theta_g}{\partial\xi}\right)_e = \left(\frac{\partial Y_i}{\partial\xi}\right)_e = \left(\frac{d\phi}{d\xi}\right)_e = 0 \quad \text{with } i = v, O, N \tag{57}$$

3.4. Ignition condition

For the solid, the ignition condition is satisfied when the rate of change of the surface temperature due to the surface oxidation reaction is equal to the rate of change of the surface temperature due to the laser heating. Mathematically it is

$$\Gamma_s = \frac{(\partial\theta_{c,\eta=1}/\partial t)_{chem}}{(\partial\theta_{c,\eta=1}/\partial t)_{laser}} \geqslant 1 \tag{58}$$

For the gas phase, a similar definition is made for every point in the calculation domain, and

$$\Gamma_{g,\xi} = \frac{(\partial\theta_{g,\xi}/\partial t)_{chem}}{(\partial\theta_{g,\xi}/\partial t)_{laser}} \geqslant 1 \tag{59}$$

4. NUMERICAL CALCULATIONS

The present numerical procedures used follow the method of lines. The spatial co-ordinates of the governing equations and the corresponding boundary conditions are discretized employing the usual central difference approximation.

$$\frac{\partial\theta_{g,i}}{\partial\xi} = \frac{\theta_{g,i+1} - \theta_{g,i-1}}{2\Delta\xi} \tag{60}$$

$$\frac{\partial\theta_{c,i}}{\partial\eta} = \frac{\theta_{c,i+1} - \theta_{c,i-1}}{2\Delta\eta} \tag{61}$$

$$\frac{\partial^2 \theta_{g,i}}{\partial \xi^2} = \frac{\theta_{g,i+1} - 2\theta_{g,i} + \theta_{g,i-1}}{\Delta \xi^2} \tag{62}$$

$$\frac{\partial^2 Y_{j,1}}{\partial \xi^2} = \frac{Y_{j,i+1} - 2Y_{j,i} + Y_{j,i-1}}{\Delta \xi^2} \tag{63}$$

$$\frac{\partial^2 \theta_{c,i}}{\partial \eta^2} = \frac{\theta_{c,i+1} - 2\theta_{c,i} + \theta_{c,i-1}}{\Delta \eta^2} \tag{64}$$

These discretized equations are then used to transform the governing equations into a system of ordinary differential equations in temporal co-ordinates for

species

$$\frac{\partial Y_{j,i}}{\partial t} = \Pi_{j,i} + \rho^2 D\left(\frac{Y_{j,i+1} - 2Y_{j,i} - Y_{j,i-1}}{\Delta \xi^2}\right) - m_s\left(\frac{Y_{j,i+1} - Y_{j,i-1}}{2\Delta \xi}\right) \quad \text{with } j = \text{v, O, N} \tag{65}$$

gas phase energy

$$\frac{\partial \theta_{g,i}}{\partial t} = \frac{\rho_g \lambda_g}{c_{p,g}}\left(\frac{\theta_{g,i+1} - 2\theta_{g,i} + \theta_{g,i-1}}{\Delta \xi^2}\right) - m_s\left(\frac{\theta_{g,i+1} - \theta_{i-1}}{2\Delta \xi}\right) + \Pi_3 \tag{66}$$

where

$$\Pi_3 = Q_{g,i} + \frac{I_0}{c_{p,g} T_e}\left(\frac{d\phi}{d\xi}\right)_i \tag{67}$$

solid energy

$$\frac{\partial \theta_{c,i}}{\partial t} = \frac{\alpha_c}{x_s^2}\left(\frac{\theta_{c,i+1} - 2\theta_{c,i} + \theta_{c,i-1}}{\Delta \eta^2}\right) \tag{68}$$

where $i = 0$ to k; k is equal to $1/\Delta\eta$ for the solid layer and k is equal to $\xi_g/\Delta\xi$ for the gas phase.

These equations are solved with the following conditions:

For $t < 0$:

$$Y_{v,i} = 0; \quad Y_{j,i} = Y_{j,e} \quad \text{with } j = \text{O, N} \tag{69}$$

$$\theta_{g,i} = \theta_{c,i} = Y_{v,c} = 0 \tag{70}$$

For $t \geqslant 0$, $\eta = 0$ ($i = 0$ for the solid):

$$\theta_{c,-1} = \theta_{c,1}; \quad \theta_{c,0} = 1 \tag{71}$$

For $t \geqslant 0$, $\eta = 1$, $\xi = \xi_s$ ($i = k$ for the solid and $i = 0$ for the gas phase):

$$\theta_{c,k} = \theta_{g,0}; \quad \left(\frac{\partial \theta_c}{\partial t}\right)_{i=k} = \left(\frac{\partial \theta_g}{\partial t}\right)_{i=0} \tag{72}$$

$$-\left(\frac{\theta_{c,k+1} - \theta_{c,k-1}}{2\Delta \eta}\right) + \Pi_1\left(\frac{\theta_{g,1} - \theta_{g,-1}}{2\Delta \xi}\right) = Q_r + Q_v - Q_c - Q_l \tag{73}$$

$$Y_{v,-1} = Y_{v,1} - \left[\frac{2\Delta \xi m_s (Y_{v,0} - 1)}{\rho_g^2 D}\right] \tag{74}$$

$$Y_{O,-1} = Y_{O,1} - \left[\frac{2\Delta \xi (m_s Y_{O,0} + \omega_c)}{\rho_g^2 D}\right] \tag{75}$$

$$Y_{N,-1} = Y_{N,1} - \left[\frac{2\Delta\xi m_s Y_{N,0}}{\rho_g^2 D}\right] \tag{76}$$

For $t \geqslant 0$, $\xi = \xi_g$ ($i = k$ for the gas phase):

$$\theta_{g,k+1} = \theta_{g,k-1}; \quad Y_{i,k+1} = Y_{i,k-1} \quad \text{with } i = \text{v, O, N} \tag{77}$$

$$\theta_{g,k} = \phi_k = 1; \quad Y_{v,k} = 0; \quad Y_{i,k} = Y_{i,e} \quad \text{with } i = \text{O, N} \tag{78}$$

The present numerical procedures use the flow quantities ($V_{i,t}$, i represents temperature, species etc.), which are known at a time level t and everywhere in the calculation domain, to advance the solution to a new level time $t + \Delta t (V_{i,t+\Delta t})$. The computer time is no longer a primary constraint with the present computer technology, consequently, one can use a very small time step Δt and $V_{i,t+\Delta t}$ can be explicitly approximated as

$$V_{i,t+\Delta t} = V_{i,t} + \frac{\partial V_{i,t}}{\partial t}\Delta t \tag{79}$$

The major problem in solving these equations is the stiffness, due to the presence of widely separated fast and slow kinetic rate equations. This requires a variable time step for the time-dependent solutions. The time step satisfying the following conditions is found to be sufficient to smooth out the solutions

$$\left[V_{i,t}\Big/\frac{\partial V_{i,t}}{\partial t}\right]E-3 \geqslant \Delta t \geqslant \left[V_{i,t}\Big/\frac{\partial V_{i,t}}{\partial t}\right]E-8 \tag{80}$$

With Δt determined from equation (80), $\Delta\eta = 0{\cdot}2$ for the solid and $\Delta\xi = 10^{-4}\,\text{g/cm}^2$ and the initial computational $\xi_g = 10^{-3}\,\text{g/cm}^2$ for the gas phase, the above ordinary differential equations in temporal co-ordinates, with the described conditions, are integrated. The integral equations for the absorption of the external radiation, equation (45) and for the gas-phase mass flux, equation (41) and the mass flux at the solid surface, equation (46), are solved using the Simpson 1/3 or combination of 1/3 and 3/8 rules. For each time step, the numerical procedures are summarized as follows:

(1) With known values of Y_v, Y_p and θ_g everywhere in the calculation domain (from $\xi = 0$ to $\xi = \xi_g$), calculate Q_g for $i = 0$ to k. Value of the absorption of the external radiation at every point, $(d\phi/d\xi)_i$, is calculated by integrating equation (45) from i to k. The gas phase mass flux, on the other hand, is calculated by integrating equation (41) from $i = 0$ to i. Values of $Y_{v,-1}$, $Y_{O,-1}$, and $Y_{N,-1}$ are calculated using equations (74)–(76). With values of θ_c from $i = 0$ to $i = k$, equation (26) is used to calculate the devolatilization rate everywhere in the solid and the surface mass flux, m_s, is calculated by integrating equation (46) from $i = 0$ to $i = k$.

(2) Using known values of $d\phi/d\xi$, ϕ and Q_g at $i = 0$; θ_g at $i = 0$ and $i = 1$; θ_c at $i = k$ and $i = k - 1$ calculate Q_c, Q_l, Q_v, Q_r. Values of $\theta_{c,k+1}$ and $\theta_{g,-1}$ are calculated using conditions given in equations (72) and (73).

(3) Using values obtained from step (1) and (2), equations (65), (66) and (68) are calculated from $i = 0$ to $i = k$. The corresponding calculation domain, ξ_g, is determined by repeating step (3) until conditions (77) and (78) are satisfied.

5. RESULTS AND DISCUSSIONS

The numerical model described above is used to simulate radiative ignition of a coal pellet. The following data are used in the simulations[11,12]: $\rho_c = 1\,\text{g/cm}^3$, $\alpha_c = 6{\cdot}5 \times 10^{-4}\,\text{cm}^2/\text{s}$, $\beta_c = 0{\cdot}8$,

$x_s = 0{\cdot}3$ cm, $A_p = 2{\cdot}06 \times 10^6$ 1/s, $E_p^* = 29{\cdot}66$, $\Delta H_p = 1550$ J/g, $A_c = 5{\cdot}075 \times 10^4$ cm/s, $E_c^* = 33{\cdot}52$, $\Delta H_c = 30\,000$ J/g for bituminous and $A_p = 4{\cdot}614 \times 10^4$ 1/s, $E_p^* = 18{\cdot}60$, $\Delta H_p = 1550$ J/g, $A_c = 4{\cdot}614 \times 10^4$ cm/s, $E_c^* = 28{\cdot}87$ for lignite coal. For the gas phase: $\rho_{g,e} = 1{\cdot}176 \times 10^{-3}$ g/cm^3, $\rho_g D = 6{\cdot}7 \times 10^{-4}$ g/cm s, $A_g \nu_v M_v = 7{\cdot}6 \times 10^{12}$ cm^3/g s, $E_g^* = 63{\cdot}68$, $\Delta H_g = 50072$ J/g and $r_{st} = 4$.

Figure 2 shows the transmittance of the radiation through the gas phase, in the presence of gases generated from the Pittsburgh bituminous coal. The data reported in Reference 1 are included for easy comparison. Data presented in Figure 2 are the ratio of the radiative flux at the coal surface to the initial radiative flux, (I_s/I_0), versus time. As shown, I_s/I_0 remained at unity during the inert-heating period which is about 0·25–1·75 ms, depending on the intensity of the radiation. As the pyrolysis process started, I_s/I_0 dropped drastically to 0·3–0·4 within a period of about 0·5 ms and then leveled off for the rest of the heating period. The results suggest that the pyrolysed gases from the coal sample can absorb a significant amount of the external radiation which can be predicted by the present numerical model.

Figure 3 shows the time histories of the surface dimensionless temperature, $\theta_{c,s}$, with and without the gas-phase absorption, for five different levels of the initial radiative fluxes. The curves showed a significant effect of the absorption of the external radiation by the devolatilization gases on both the surface heating and the gas-phase heating. When the absorption in the gas phase was excluded, the surface temperature increased rapidly with time during the initial heating period. After the pyrolysis became active, the surface temperature continued to increase slowly and then leveled off for the rest of the heating period. When the absorption of the radiation in the gas phase was included, the same rates of the surface temperature rise during the initial heating period was obtained. However, after the pyrolysis became active, the surface temperature started to decline.

Figure 4 shows the dimensionless temperature profiles, θ_g, in the gas-phase region. For the non-absorption case (the solid lines) the temperature profiles, obtained with and without the

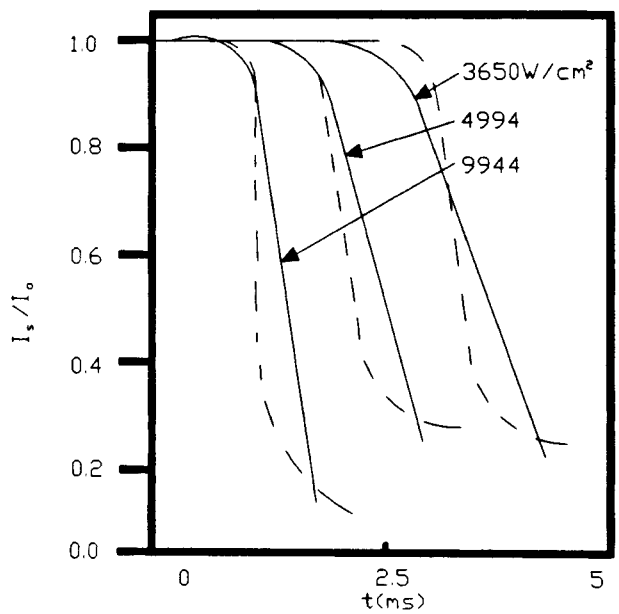

Figure 2. Calculated and measured I_s normalized by I_0 as function of time for three levels I_0 (bituminous coal, $A_p = 2{\cdot}06 \times 10^6$ 1/s, $E_p^* = 29{\cdot}66$, $\beta_g = 1{\cdot}0$ 1/cm; (------) measured,(——) calculated)

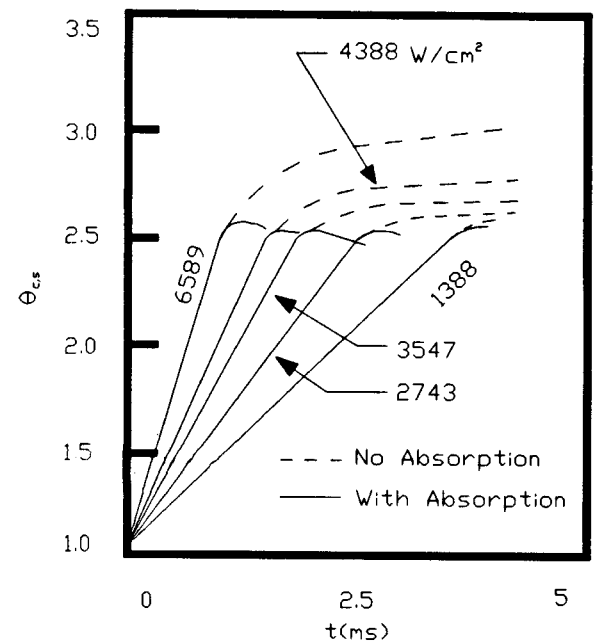

Figure 3. Calculated $\theta_{c,s}$ as function of time with and without the gas-phase absorption (bituminous coal, $A_p = 2{\cdot}06 \times 10^6$ 1/s, $E_p^* = 29{\cdot}66$, $\beta_g = 1{\cdot}0$ 1/cm)

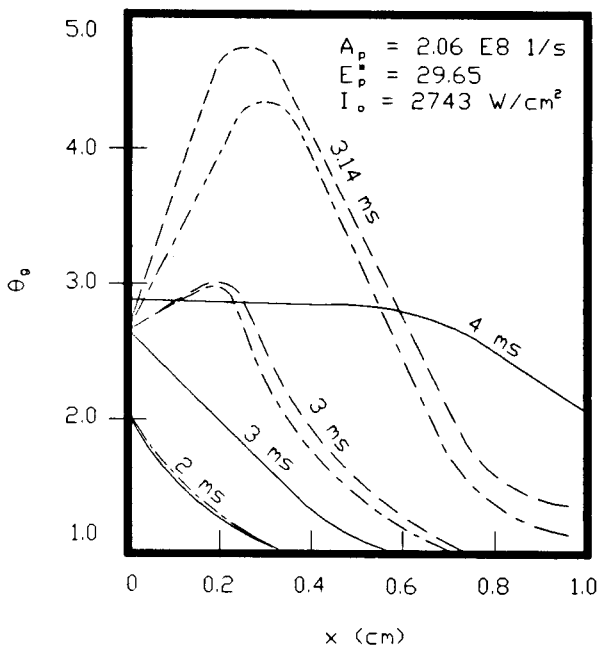

Figure 4. Gas-phase dimensionless temperature profiles as a function of space and time (bituminous coal, (------) with absorption, $\beta_g = 1$ 1/cm, and chemical reaction, (——·——) with absorption $\beta_g = 1$ 1/cm, and no chemical reaction, (——) without absorption and with/without chemical reaction)

gas-phase chemical reactions, are the same. The highest temperature was always at the surface and decreased monotonically toward the edge of the calculation domain. This indicates that chemical reactions in the gas phase are not active enough so as to contribute significantly to the gas-phase heating leading to ignition.

For the absorption case (the dashed and dash-dotted lines), however, there was a sudden rise in the gas-phase temperature just after the onset of the devolatilization. The gas-phase ignition was observed at time $t = 3{\cdot}14$ ms, where the curve, obtained without the gas-phase reactions (dash-dotted line), reached its maximum temperature of about 1200 K ($\theta_g = 4{\cdot}0$) while the curve, obtained with the gas-phase reactions (dashed line), had the maximum temperature of about 1380 K ($\theta_g = 4{\cdot}6$).

The surface ignition time and the gas-phase ignition time are shown in Figures 5 and 6, respectively. For radiative fluxes ranging from 2500 to 7000 W/cm^2, the ignition of lignite and subbituminous coals was seen as an integration of two consecutive ignition modes: The surface ignition occurred first and it was then followed by the ignition of the volatile gases in the gas-phase region. However, only a single gas-phase ignition mode was observed for Pittsburgh bituminous coal. Included in these figures are the measured ignition times reported in Reference 1. A good agreement between the measured and the calculated ignition times was obtained. The ability of the numerical model to predict the ignition modes and the magnitude of the ignition times for the coals seems to be due to the inclusion of all processes, associated with the radiative ignition of coals.

The effects of the surface ignition reaction activation energy and the devolatilization activation energy on the gas-phase and the surface ignition times are shown in Figure 7. It is clear that for

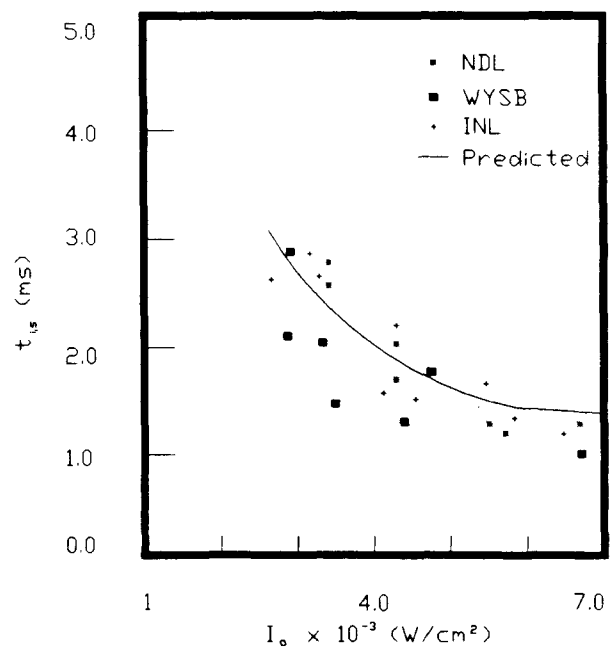

Figure 5. Measured and calculated surface ignition times as a function of I_0, ($E_p^* = 28$; $E_c^* = 12$; $\beta_g = 1{\cdot}0$ 1/cm; NDL: North Dakota lignite; WYSB: Wyoming subbituminous; INL: Indiana lignite)

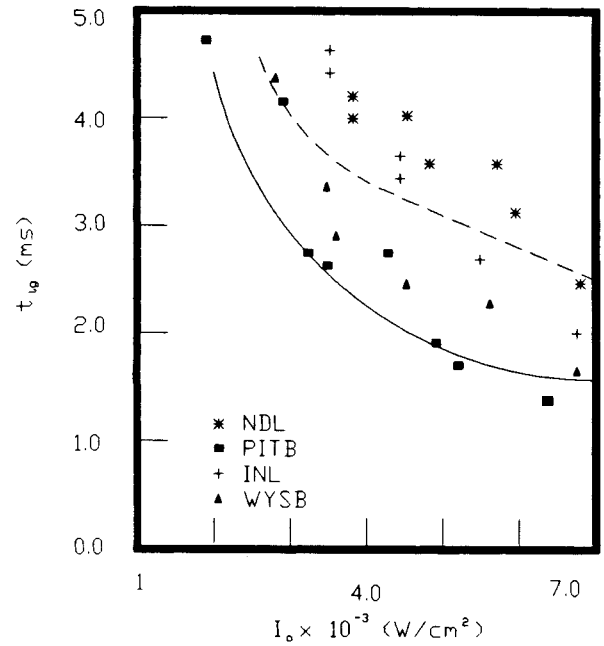

Figure 6. Measured and calculated gas-phase ignition times as a function of I_0 ($\beta_g = 1{\cdot}0$ 1/cm; (-----) predicted lignite; $E_p^* = 28$; $E_c^* = 12$; (——) predicted, bituminous; NDL: North Dakota lignite; WYSB: Wyoming subbituminous; INL: Indiana lignite; PITB: Pittsburgh bituminous)

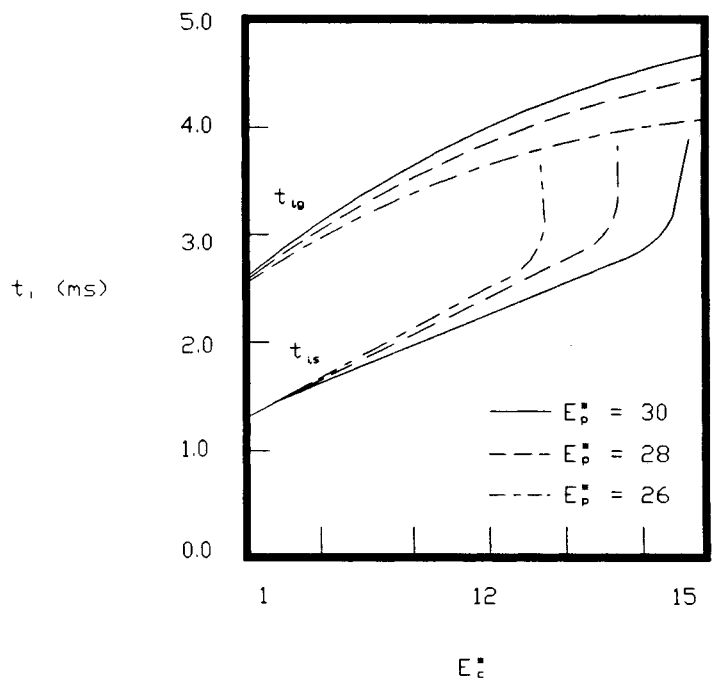

Figure 7. Effect of the surface ignition reaction activation energy, E_c^*, on ignition times ($I_0 = 3632$ W/cm^2; $E_g^* = 63{\cdot}68$; $\beta_g = 1{\cdot}0$ 1/cm)

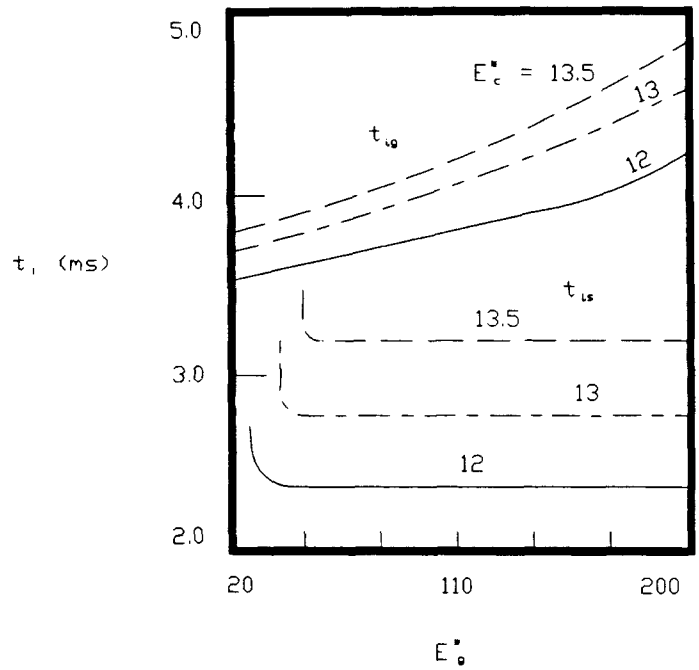

Figure 8. Effect of the gas-phase reaction activation energy, E_g^*, on ignition times ($I_0 = 3632\,W/cm^2$; $E_p^* = 28$; $\beta_g = 1{\cdot}0\,1/cm$)

each value of the devolatilization activation energy there exists an upper limit of the surface ignition reaction activation energy, below which, two ignition modes are present. However, when the surface ignition reaction activation energy is above this limit, the surface ignition is not obtainable and only the gas-phase ignition is possible.

Figure 8 shows the gas-phase and the solid ignition times as a function of the gas-phase activation energy. There exists a lower limit of the gas-phase activation energy, above which, the surface ignition was obtained and this was followed by the gas-phase ignition. The existence of the lower limit of the gas-phase activation energy is due to the fact that although the gas-phase reaction is not active at low temperature and low concentration of volatile gases in the initial stage, the oxidizer is consumed rapidly due to the high value of the stoichiometry ratio and the low value of the activation energy. As a result, the amount of the oxidizer coming to the coal surface is reduced. In the later stage, as the devolatilization becomes active, volatile gases act like a shield preventing the oxidizer from reaching the coal surface. Thus the lack of oxidizer at the coal surface, due to the low value of the gas-phase activation energy in the initial stage and due to the present of the volatile gases in the later stages of the ignition event, prevents the surface ignition from occurring.

6. CONCLUSIONS

A numerical model of the radiative ignition of a pyrolysing solid fuel was presented. The model included essentially all processes associated with the radiative ignition of a pyrolysing solid fuel and it was able to predict the two ignition modes and the amount of the external radiation

absorbed by the volatile gases reported in Reference 1. The absorption of the external radiation by the volatile gases was found to be a very important process which led to the ignition of the volatile gases in the gas phase. Such a process also significantly controls processes occurring at the target surface, in the gas phase in the initial stage, and during the combustion of the residual gases in the final stage.

A sensitivity analysis, where the kinetic parameters of the reactions involved, was also carried out. This analysis established an upper limit of the surface activation energy and a lower limit of the gas-phase activation energy. Within these limits, the radiative ignition of coals was an integration of two consecutive ignition modes: The surface ignition occurs first when it was followed by the gas-phase ignition. Beyond these limits, the gas-phase ignition was the only ignition mode to prevail.

APPENDIX

Nomenclature

A_g pre-exponential factor of gas-phase combustion reaction ($m^3/kg^2\,kmol\,s$)
A_p pre-exponential factor of volumetric pyrolysis reaction (1/s)
A_c pre-exponential factor of surface combustion reaction (m/s)
c_p specific heat (kJ/kg K)
D diffusion coefficient (m^2/s)
E activation energy (kJ/kmol)
E^* dimensionless activation energy
I radiative energy flux ($kJ/m^2\,s$)
I_0 initial radiative energy flux ($kJ/m^2\,s$)
I_0^* the upper limit of the radiative energy flux ($kJ/m^2\,s$)
M molecular weight (kg/kmol)
m_s pyrolysis mass flux at the solid surface ($kg/m^2\,s$)
R universal gas constant (kJ/kmol K)
t time (s)
$t_{i,s}$ surface ignition time (s)
$t_{i,g}$ gas-phase ignition time (s)
T temperature (K)
T_e ambient temperature (K)
u gas velocity (m/s)
x x-co-ordinate (m)
x_s initial thickness of the solid (m)
x_g initial edge of the gas phase (m)
Y mass fraction
$Y_{v,c}^*$ volatile fraction in the solid

Greek symbols

α_c solid thermal diffusivity (m^2/s)
β_c absorption coefficient of the solid
β_g absorption coefficient of the gas phase (1/m)
Γ_s surface ignition condition
$\Gamma_{g,\xi}$ gas-phase ignition condition
ΔH_v heat of pyrolysis of the solid (kJ/kg)

ΔH_c heat surface combustion reaction (kJ/kg)
ΔH_g heat of gas-phase combustion reaction (kJ/kg)
η dimensionless distance co-ordinates
θ dimensionless temperature
θ_i dimensionless ignition temperature
λ thermal conductivity (kJ/m K s)
ν_i stoichiometric coefficient of species i
ξ stream function
ρ density (kg/m^3)
σ Stefan–Boltzmann constant (kJ/m^2 s K^4)
ϕ dimensionless intensity of the radiative heat flux
ω_v gas-phase reaction rate (kg/m^3 s)
ω_c surface reaction rate (kg/m^2 s)
ω_p pyrolysis rate (1/s)

Subscripts

c solid
e ambient condition
g gas
i species i, ignition
N inert gas
O oxygen
p pyrolysis, product
s surface
v volatile

REFERENCES

1. T. X. Phuoc, M. P. Mathur and J. M. Ekmann, 'High-energy Nd-Yag laser ignition of coals: experimental observations', *Combust. Flame*, **93,** 19–30 (1993).
2. T. Kashiwagi, 'Experimental observation of radiative ignition mechanisms', *Combust. Flame*, **34,** 231–244 (1979).
3. T. Kashiwagi, 'Effects of attenuation of radiation on surface temperature for radiative ignition', *Combust. Sci. Technol.*, **20,** 225–234 (1979).
4. T. Kashiwagi, 'A radiative ignition model of a solid fuel', *Combust. Sci. Technol.*, **8,** 225–236 (1974).
5. S. H. Park and C. L. Tien, 'Radiative induced ignition of solid fuels', *Int. J. Heat Mass Transfer*, **33,** 1511–1520 (1990).
6. C. Di Blasi, S. Crescitelli, G. Russo and G. Cinque, 'Numerical model of ignition processes of polymeric materials including gas-phase absorption of radiation', *Combust. Flame*, **83,** 333–344 (1991).
7. B. Amos and A. C. Fernandez-Pello, 'Model of ignition and flame development on a vaporizing combustible surface in a stagnation point flow: ignition by vapor fuel absorption', *Combust. Sci. Technol.*, **62,** 331–343 (1988).
8. P. Durbetaki and T. X. Phuoc, 'Numerical study of laser-induced ignition of coals', in R. W. Lewis, (ed.), *Numerical Methods in Thermal Problems*, Vol. 8, Pineridge Press, Swansea, U.K., 1993, pp. 1310–1321.
9. X. Li and P. Durbetaki, 'Ignition of a vertically oriented solid fuel under radiative heating', in R. W. Lewis (ed.), *Numerical Methods in Thermal Problems*, Vol. 8, Pineridge Press, Swansea, U.K., 1993, pp. 782–793.
10. J. R. Koski an P. Durbetaki, 'Numerical solution of the radiation induced ignition of solid fuels', in R. W. Lewis (ed.), *Numerical Methods in Thermal Problems*, Vol. 8, Pineridge Press, Swansea, U.K., 1993, pp. 733–744.
11. T. X. Phuoc, M. P. Mathur, J. M. Ekmann and P. Durbetaki, 'High-energy Nd-Yag laser ignition of coals: modeling analysis', *Combust. Flame*, **93,** 349–362 (1993).
12. K Annamalai and P. Durbetaki, 'A theory on transition of ignition phase of coal particles', *Combust. Flame*, **29,** 193–208 (1977).